

UC Irvine

UC Irvine Previously Published Works

Title

Third-harmonic generation from Mie-type resonances of isolated all-dielectric nanoparticles.

Permalink

<https://escholarship.org/uc/item/3rn144dt>

Journal

Philosophical Transactions of the Royal Society A: Mathematical, Physical and Engineering Sciences, 375(2090)

ISSN

1364-503X

Authors

Melik-Gaykazyan, Elizaveta  
Shcherbakov, Maxim  
Shorokhov, Alexander  
et al.

Publication Date

2017-03-28

DOI

10.1098/rsta.2016.0281

Peer reviewed

## Research



**Cite this article:** Melik-Gaykazyan EV, Shcherbakov MR, Shorokhov AS, Staude I, Brener I, Neshev DN, Kivshar YS, Fedyanin AA. 2017 Third-harmonic generation from Mie-type resonances of isolated all-dielectric nanoparticles. *Phil. Trans. R. Soc. A* **375**: 20160281.  
<http://dx.doi.org/10.1098/rsta.2016.0281>

Accepted: 1 September 2016

One contribution of 15 to a theme issue 'New horizons for nanophotonics'.

### Subject Areas:

nanotechnology, optics

### Keywords:

nonlinear optics, third-harmonic generation, silicon nanoparticles, optical magnetism, Mie scattering

### Author for correspondence:

Andrey A. Fedyanin  
e-mail: [fedyanin@nanolab.phys.msu.ru](mailto:fedyanin@nanolab.phys.msu.ru)

# Third-harmonic generation from Mie-type resonances of isolated all-dielectric nanoparticles

Elizaveta V. Melik-Gaykazyan<sup>1</sup>, Maxim R. Shcherbakov<sup>1</sup>, Alexander S. Shorokhov<sup>1</sup>, Isabelle Staude<sup>2,3</sup>, Igal Brener<sup>4</sup>, Dragomir N. Neshev<sup>2</sup>, Yuri S. Kivshar<sup>2</sup> and Andrey A. Fedyanin<sup>1</sup>

<sup>1</sup>Faculty of Physics, Lomonosov Moscow State University, Moscow 119991, Russia

<sup>2</sup>Nonlinear Physics Centre, Research School of Physics and Engineering, The Australian National University, Canberra, Australian Capital Territory 2601, Australia

<sup>3</sup>Institute of Applied Physics, Abbe Center of Photonics, Friedrich Schiller University Jena, 07745 Jena, Germany

<sup>4</sup>Center for Integrated Nanotechnologies, Sandia National Laboratories, Albuquerque, NM 87185, USA

EVM-G, 0000-0001-7633-2376

Subwavelength silicon nanoparticles are known to support strongly localized Mie-type modes, including those with resonant electric and magnetic dipolar polarizabilities. Here we compare experimentally the efficiency of the third-harmonic generation from isolated silicon nanodiscs for resonant excitation at the two types of dipolar resonances. Using nonlinear spectroscopy, we observe that the magnetic dipolar mode yields more efficient third-harmonic radiation in contrast to the electric dipolar (ED) mode. This is further supported by full-wave numerical simulations, where the volume-integrated local fields and the directly simulated nonlinear response are shown to be negligible at the ED resonance compared with the magnetic one.

This article is part of the themed issue 'New horizons for nanophotonics'.

## 1. Introduction

In nanoplasmonics, noble metal nanoparticles allow for shaping local electromagnetic fields on demand, an ability that has spawned many applications as well as inspired a vast amount of research in photonics [1]. Having control over the local fields is crucial for nonlinear-optical applications where frequency conversion, self-action and all-optical switching are highly sensitive to the structure geometry and the excited electromagnetic modes [2]. Apart from the electric dipolar (ED) modes in simple geometries such as spheres [3,4] or dipole antennas [5,6], the modes with considerable magnetic dipolar (MD) moment [7–9] were extensively studied in the nonlinear-optical regime [10], being mainly associated with metamaterials and ‘metamolecules’ supporting optically induced magnetic response. Examples include the second- and third-harmonic (TH) generation in split-ring resonators [11], fishnet metamaterials [12,13], split-hole cavities [14] and nanosandwiches [15]. A special contribution of MD modes to the nonlinear multipolar response of metasurfaces was indicated [15–17].

Observation of MD modes [18] in arrays of dielectric resonators [19] and, in particular, silicon nanoparticles [20,21] was an important step towards low-loss all-dielectric nanophotonics [22]. Having extremely low absorption in the near-IR spectral region, silicon is even more attractive in the nonlinear regime [23–25]. Previously, we have shown that MD modes can substantially improve the nonlinear response of silicon nanodiscs [26,27] and their oligomers [28,29]. Apart from the fact that the MD mode is often the lowest-order mode of a high-index subwavelength spherical or disc-like nanoparticle, it remains unclear whether there is any further advantage of using this mode for nonlinear conversion processes when compared with ED or higher-order modes.

In this paper, we compare the nonlinear effects produced by optically isolated silicon nanoparticles being pumped at their ED and MD resonances, by employing third-harmonic generation (THG) spectroscopy technique. As depicted schematically in figure 1*a*, we observe that exciting the MD resonance leads to a large THG yield compared with the case of ED resonance because of the stronger field confinement within the nanodisc for the MD resonance. This is supported by rigorous numerical calculations of the electric field distributions that show strong enhancement of the overall local field for the MD mode, and rigorous numerical simulations of the nonlinear-optical response.

## 2. Methods

### (a) Samples

Nanodisc arrays are fabricated starting with a silicon-on-insulator (SOI) wafer, produced by Soitec, using electron-beam lithography and reactive-ion etching processes. The top (100)-cut Si layer of the wafer is 260 nm thick. We consider two square  $400 \times 400 \mu\text{m}^2$  arrays distinguished by disc diameter values of  $d = 345$  and 360 nm, respectively. The nanodisc lattice spacing is  $p = 2.85 \mu\text{m}$  for all the diameters. As opposed to our previous results on nonlinear spectroscopy of Si metasurfaces [26], such a period value allows for studying isolated nanodiscs owing to negligible optical coupling through near-field interactions ( $d \ll p$  and  $\lambda < p$ ). The choice of the nanodisc diameter and height specifies the MD and ED resonance wavelengths [30]. A scanning electron microscopy image of a 360 nm disc array part is shown in figure 1*b*.

### (b) Nonlinear spectroscopy

In order to study the nonlinear-optical response of the nanodiscs and to clarify the roles played by ED and MD resonances in the harmonic generation process, we conduct nonlinear THG spectroscopy measurements. An optical parametric oscillator (Angewandte Physik & Elektronik GmbH OPO PP Automatic; 200 fs pulses) is pumped by a Ti:sapphire oscillator (Coherent Chameleon Ultra II, repetition rate 76 MHz) and tuned in the range of 1.0–1.5  $\mu\text{m}$ . The beam

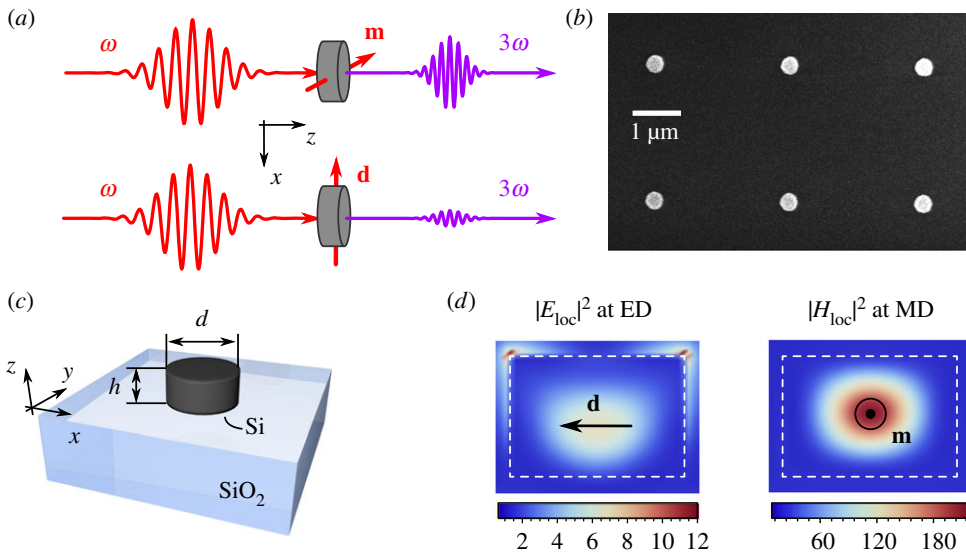


**Figure 1.** (a) Third-harmonic generation from electric ( $\mathbf{d}$ ) and magnetic ( $\mathbf{m}$ ) dipolar resonances of individual silicon nanodiscs;  $\mathbf{m}$  and  $\mathbf{d}$  are macroscopically averaged main multipolar moments of the nanodisc. (b) Scanning electron micrograph of a sample under study. (c) Schematic of the structure with dimensions and axes defined. (d) Maps of the local electric field at the ED resonance and magnetic field at the MD resonance proving the multipolar moments of the resonances. The maps are given in the central  $xz$  section of the disc for  $h = 260 \text{ nm}$ ,  $d = 360 \text{ nm}$  and  $\lambda = 1.030$  and  $1.296 \mu\text{m}$  for the ED and MD resonances, respectively. (Online version in colour.)

polarization is conditioned by a pair of Glan-laser prisms. The waist diameter is set at  $11 \mu\text{m}$  by an aspheric lens. The beam is focused from the back of the sample, and the transmitted third-harmonic beam is measured. The full thickness of the SOI wafer ( $500 \mu\text{m}$ ) is comparable to the waist depth. The resulting peak intensity reached values of about  $1 \text{ GW cm}^{-2}$  in the sample plane. For the preliminary focusing at the area of interest, a CCD camera and a halogen lamp are used. The transmitted and collimated THG signal is selected by a set of blue filters and detected by a photomultiplier tube connected to a lock-in amplifier. The periodic arrangement formed a square diffraction pattern; we deliberately collect the zeroth-transmitted order for measuring the forward-scattered signal only. This signal is proven to be of the TH origin by checking its cubic dependence on the pump power and by direct measurements of its spectrum by a spectrometer. It has been also verified that the THG beam is polarized parallel to the orientation of the pump beam polarization. It should be pointed out that the penetration depth of the TH field into silicon does not exceed the nanodisc height.

The key feature of our approach is the possibility to cancel out all the sample-irrelevant contributions to the measured spectra, such as pulse duration and power variations, along with spectral features of the set-up itself, as well as the dispersion of  $\chi^{(3)}$  for bulk silicon. Our nonlinear spectroscopy set-up has an option for measuring the linear transmittance spectra by focusing white light to a  $20 \mu\text{m}$  wide spot on the sample plane and consecutively measuring its spectrum using an IR spectrometer.

All measurements are carried out under normal incidence and with all the beams polarized along the side of the sample periodicity cell. The numerical aperture for the pump beam was equal to 0.15.

### (c) Estimation of third-harmonic output via local fields integration

The fact of the higher TH yield upon pumping the MD resonances if compared with the ED resonance is supported by estimating the overall nonlinear polarization within the nanodiscs. This has been done by integrating the local fields over the volume of the nanodisc.

To simulate the nanodisc response to external radiation, we implement a model using FDTD SOLUTIONS software by Lumerical Solutions, Inc. This model includes a plane wave pulse with a wide spectral range (0.8–1.4  $\mu\text{m}$ ) as an external radiation source located inside the silica substrate. For a Si nanodisc, dimensions are set equal to those of the experiment, namely the height is 260 nm, and the diameter is 360 nm. After calculating the electromagnetic field components outside and inside the disc, we integrate the Cartesian components of the time-averaged electric field:

$$|E_{\text{int},i}(\lambda)|^2 = \int_{V_{\text{disc}}} |E_i(\mathbf{r}, \lambda)|^2 d\mathbf{r}, \quad (2.1)$$

and the absolute value of the squared total field:

$$|E_{\text{int}}(\lambda)|^2 = \int_{V_{\text{disc}}} (|E_x(\mathbf{r}, \lambda)|^2 + |E_y(\mathbf{r}, \lambda)|^2 + |E_z(\mathbf{r}, \lambda)|^2) d\mathbf{r}, \quad (2.2)$$

over the disc volume  $V_{\text{disc}}$ . The spectral features of the source are taken into account by a normalization procedure. The disc is considered isolated owing to the perfectly matched layers set as boundary conditions.

#### (d) Numerical simulations of third-harmonic output

Our nonlinear spectroscopy result is compared with direct numerical calculations of THG response. We consider the same model of the nanodisc on the silica substrate using FDTD SOLUTIONS software by Lumerical Solutions, Inc. The material of the disc was augmented by a constant isotropic nonlinear susceptibility  $\chi^{(3)}$ . The dispersion of the nonlinear susceptibility as well as its tensorial nature are not taken into account for our estimations of TH output. For each wavelength, the pump was simulated to be a plane wave pulse with a relatively narrow spectral width of 5 nm, which was close to the experimental value. The nonlinear signal was recorded in the spectral vicinity of the respective tripled frequency as detected by a two-dimensional transmission monitor and integrated as a function of the two coordinates and frequency. To be able to compare our experimental and numerical results, we also calculate the THG response from a bulk Si substrate. It was made by considering a semi-infinite bulk Si material with the same nonlinear susceptibility and periodic boundary conditions. The final data represent the ratio of the THG responses calculated for an isolated disc  $I_{3\omega}^{\text{disc}}$  and bulk silicon  $I_{3\omega}^{\text{bulk Si}}$ , i.e.  $I_{3\omega}^{\text{disc}}/I_{3\omega}^{\text{bulk Si}} + 1$ . For the sake of simplicity, we do not consider the possible interference effects in the 2  $\mu\text{m}$  silica layer.

### 3. Results and discussion

Our experimental results are summarized in figure 2*a,b*. For the linear optical response characterization, we normalize the white-light transmittance spectrum by the spectrum of the nearby substrate area measured under the same conditions. We observe two dips in the normalized transmittance spectra. The dips correspond to the ED resonance found at shorter wavelengths, and MD resonance is found at longer wavelengths; this interpretation is supported by the corresponding numerical calculations summarized below. A difference in the position of the magnetic resonance wavelength observed for the two samples is about 30 nm, and this is more substantial for the magnetic rather than for electric resonance owing to the sensitivity of the former to the disc diameter [30].

The measured THG spectra are shown in figure 2*a,b* with black dots and corresponding error bars. First, despite the simultaneous illumination of both the nanodisc arrays and the bulk silicon SOI substrate, we observe a significant THG enhancement from the nanodiscs compared with the bulk silicon THG. The enhancement peak corresponds to the wavelength of the MD resonance. Moreover, the THG enhancement is highly pronounced at the MD resonance wavelength (this was also observed in our previous work for optically coupled nanodiscs [26]), whereas at the ED resonance, there is no significant enhancement. The THG line is expectedly narrower than that of the transmittance spectrum. A small, yet persistent, red shift of the central THG resonance

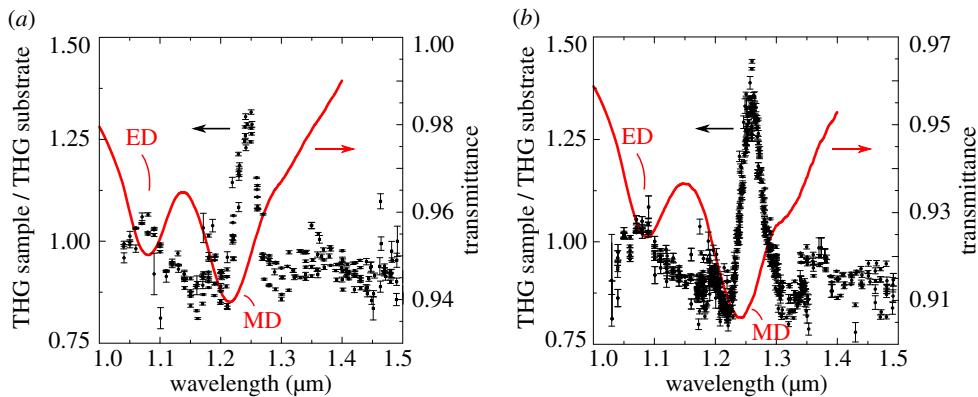


**Figure 2.** Experimental results. Spectra of the third-harmonic generation (dots and error bars) and the corresponding linear transmittance (red solid curves) for nanodiscs 345 nm (a) and 360 nm (b) in diameter, respectively. (Online version in colour.)

wavelength is observed with respect to the transmittance dip. Such spectral shifts have been already demonstrated in previous nonlinear spectroscopy research [31,32]. They can be attributed both to dispersion of the material at the TH wavelength and to the fact that the local fields are not necessarily at their maximum at the transmittance dip; the latter statement is supported numerically below. The maximum enhancement is defined as a ratio of the normalized THG signal (the THG intensity from the discs, located on the substrate, divided by the THG intensity from the substrate, i.e.  $|\mathbf{E}_{3\omega}^{\text{disc}} + \mathbf{E}_{3\omega}^{\text{sub}}|^2 / |\mathbf{E}_{3\omega}^{\text{sub}}|^2$ ) to the inverse value of the relative nanodisc area  $4p^2/\pi d^2$  being around 30, which is consistent with our previous findings for sparsely arranged oligomers [28].

In order to elucidate the observed asymmetry in the efficiencies between the THG at the magnetic resonance versus that at the electric resonance, we calculate numerically the volume-integrated local electromagnetic fields within the disc. It is known that the nonlinear polarization depends strongly on the strength of the local electromagnetic field; in the case of the scalar nonlinear susceptibility  $\chi^{(3)}$  [33]:

$$\tilde{P}(t) = \chi^{(3)} \tilde{E}_{\text{local}}^3(t). \quad (3.1)$$

Here,  $\tilde{P}(t)$  is the induced third-order nonlinear polarization that results in the TH radiation in the far field. Although the mechanism that leads to the resulting far-field THG pattern is complicated, here we rely on the assumption that the local field value  $E_{\text{local}}$  is the dominant mechanism for the overall TH response. First, using finite-difference time-domain (FDTD) approach, we calculate  $\mathbf{E}_{\text{local}}(\mathbf{r}, \lambda)$  maps within the single silicon nanodisc situated on a silica substrate. The dimensions of the nanodiscs are taken from the experimental values ( $h = 260$  nm,  $d = 360$  nm). Then, the time-averaged fields are integrated over the volume of the nanodisc; the integrated values  $\mathbf{E}_{\text{int}}(\lambda)$  give a direct estimate of how much TH should be detected at a particular pump wavelength  $\lambda$ . The spectra of the volume-integrated local fields are provided in figure 3a. Here, the components and the absolute field value squared are plotted in the spectral range of three low-order Mie-type resonances that carry MD, ED and magnetic quadrupolar (MQ) [20,21] moments. From the spectra of the integrated local fields, we observe that the ED resonance has little contribution to the overall local field enhancement. The strongest nonlinear response is, therefore, expected at the MD and MQ resonances. This observation is also supported by the corresponding local field maps that are provided in figure 3b for MD at  $\lambda = 1.296$   $\mu\text{m}$ , for ED at  $\lambda = 1.03$   $\mu\text{m}$  and for MQ at  $\lambda = 0.896$   $\mu\text{m}$ , respectively. The largest value of the local electric field is obtained at the MQ resonance. If one compares the ED and MD modes, then the peak local field values within the nanodisc are in favour of the MD resonance: the normalized  $E$ -field peaks at 2.71 at the ED resonance versus 3.20 at the MD resonance. In addition, the overall volume covered by hotspots

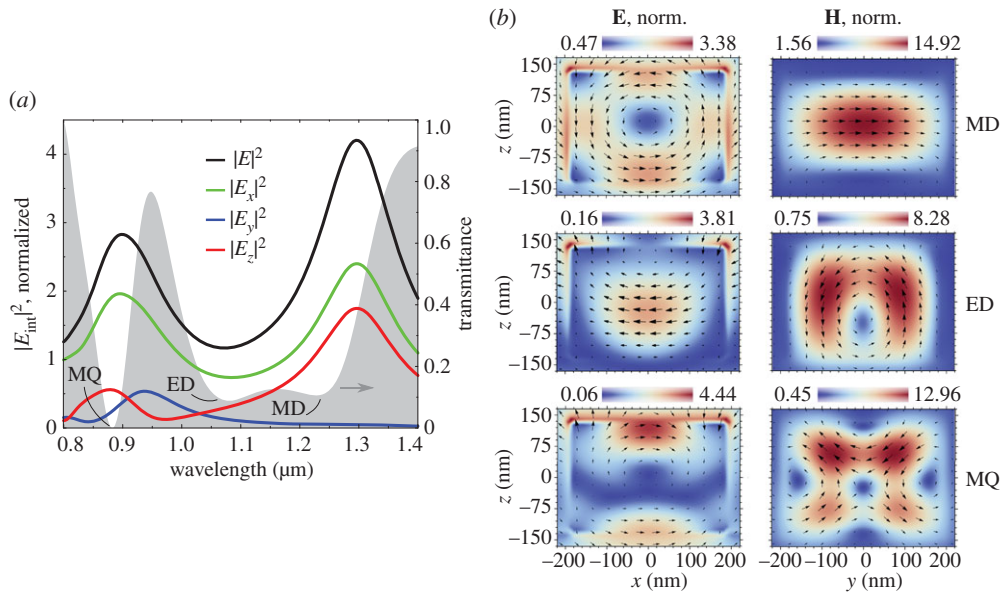


**Figure 3.** Results of the FDTD numerical calculations. (a) Absolute squared electric field integrated over the volume of the nanodisc; height is 260 nm, diameter is 360 nm. Different field components are indicated with differently coloured curves:  $E_x$  is given in green,  $E_y$  in blue,  $E_z$  in red and total field in black. The gray-shaded area denotes the calculated transmittance spectrum. (b) Field distributions in the central sections of the nanodisc at the MD resonance ( $\lambda = 1.296 \mu\text{m}$ ), ED resonance ( $\lambda = 1.03 \mu\text{m}$ ) and MQ resonance ( $\lambda = 0.896 \mu\text{m}$ ). (Online version in colour.)

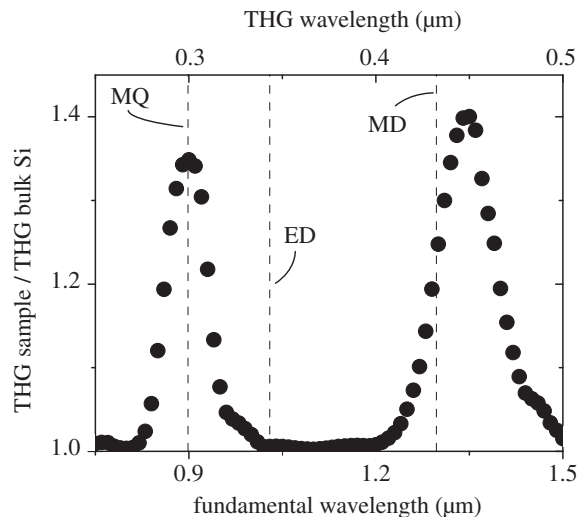


**Figure 4.** Results of the FDTD numerical calculations for the THG response from an isolated nanodisc. Nanodisc height and diameter are 260 and 360 nm, respectively.

is visually larger for the MD mode. Therefore, the experimentally observed enhanced THG at the MD resonance, when compared with the THG output at the ED resonance, can be validated by a simple local-field hypothesis. These results make the MD resonances of high-index nanoparticles very relevant to nonlinear-optical applications in nanophotonics.

Moreover, direct numerical simulations suggest that the THG response takes place at the MD resonance of an isolated silicon disc, whereas at the ED resonance the nonlinear signal appears to be rather weak (figure 4). The calculations provide the same value of the TH intensity enhancement from the nanostructured area in comparison with the intensity from the substrate, which is observed in the experiment (figure 2*b*). A significant enhancement of nonlinear process efficiency is also predicted at the MQ resonance; an experimental verification of this fact could be interesting for ultraviolet photonics applications. An apparent red spectral shift of the TH signal with respect to the spectral position of the MD mode-associated dip is consistent with the integrated electric field in figure 3.

## 4. Conclusion

We have studied the THG from silicon nanodiscs at their Mie-type ED and MD resonances. The enhanced upconversion efficiency at the MD resonance of the nanodiscs has been observed owing to the strong field confinement, whereas the ED resonance yielded almost no nonlinear conversion. The experimental findings have been supported by rigorous nonlinear numerical calculations, where considerably lower average local field density and overall THG has been detected at the electric resonance, when compared with the magnetic resonance. We believe that these results provide an important step towards the better understanding of artificial resonant all-dielectric nanostructures and their nonlinear-optical response at the nanoscale.

**Authors' contributions.** All the authors contributed to conceptualizing this paper. E.V.M. carried out numerical simulations and experiments. E.V.M. and M.R.S. wrote the first draft. E.V.M., M.R.S. and A.S.S. chose the methods and constructed the experimental set-up. I.S. and I.B. fabricated the sample. I.S., D.N.N., I.B., Y.S.K. and A.A.F. revised the manuscript. All the authors gave final approval for publication.

**Competing interests.** The authors have no competing interests.

**Funding.** The authors acknowledge financial support from Russian Foundation for Basic Research (grant nos. 16-29-11811 and 16-02-01092) and the Australian Research Council. This work was performed, in part, at the Center for Integrated Nanotechnologies, an Office of Science User Facility operated for the US Department of Energy (DOE) Office of Science. Sandia National Laboratories is a multiprogramme laboratory managed and operated by Sandia Corporation, a wholly owned subsidiary of Lockheed Martin Corporation, for the US Department of Energy's National Nuclear Security Administration under contract DE-AC04-94AL85000.

**Acknowledgements.** The authors thank Ivan Iorsh and Daria Smirnova for fruitful discussions.

## References

1. Maier SA. 2007 *Plasmonics: fundamentals and applications*. New York, NY: Springer Science + Business Media.
2. Kauranen M, Zayats AV. 2012 Nonlinear plasmonics. *Nat. Photonics* **6**, 737–748. (doi:10.1038/nphoton.2012.244)
3. Lippitz M, Dijk MA, Orrit M. 2005 Third-harmonic generation from single gold nanoparticles. *Nano Lett.* **5**, 799–802. (doi:10.1021/nl0502571)
4. Liu TM, Tal SP, Yu CH, Wen YC, Chu SW, Chen LJ, Prasad MR, Lin KJ, Sun CK. 2006 Measuring plasmon-resonance enhanced third-harmonic  $\chi^{(3)}$  of Ag nanoparticles. *Appl. Phys. Lett.* **89**, 112–114. (doi:10.1063/1.2240738)
5. Aouani H, Rahmani M, Navarro-Cía M, Maier SA. 2014 Third-harmonic-upconversion enhancement from a single semiconductor nanoparticle coupled to a plasmonic antenna. *Nat. Nanotechnol.* **9**, 290–294. (doi:10.1038/nnano.2014.27)
6. Metzger B, Hentschel M, Schumacher T, Lippitz M, Ye X, Murray CB, Knabe B, Buse K, Giessen H. 2014 Doubling the efficiency of third harmonic generation by positioning ITO nanocrystals into the hot-spot of plasmonic gap-antennas. *Nano Lett.* **14**, 2867–2872. (doi:10.1021/nl500913t)
7. Shalaev VM. 2007 Optical negative-index metamaterials. *Nat. Photonics* **1**, 41–48. (doi:10.1038/nphoton.2006.49)

8. Dolling G, Enkrich C, Wegener M, Zhou JF, Soukoulis CM, Linden S. 2005 Cut-wire pairs and plate pairs as magnetic atoms for optical metamaterials. *Opt. Lett.* **30**, 3198–3200. (doi:10.1364/OL.30.003198)
9. Pshenay-Severin E, Hübner U, Menzel C, Helgert C, Chipouline A, Rockstuhl C, Tünnermann A, Lederer F, Pertsch T. 2009 Double-element metamaterial with negative index at near-infrared wavelengths. *Opt. Lett.* **34**, 1678–1680. (doi:10.1364/OL.34.001678)
10. Klein MW, Enkrich C, Wegener M, Linden S. 2006 Second-harmonic generation from magnetic metamaterials. *Science* **313**, 502–504. (doi:10.1126/science.1129198)
11. Klein MW, Wegener M, Feth N, Linden S. 2007 Experiments on second- and third-harmonic generation from magnetic metamaterials. *Opt. Express* **15**, 5238–5247. (doi:10.1364/OE.15.005238)
12. Kim E, Wang F, Wu W, Yu Z, Shen YR. 2008 Nonlinear optical spectroscopy of photonic metamaterials. *Phys. Rev. B* **78**, 113102. (doi:10.1103/PhysRevB.78.113102)
13. Shorokhov AS, Okhlopkov KI, Reinhold J, Helgert C, Shcherbakov MR, Pertsch T, Fedyanin AA. 2016 Ultrafast control of third-order optical nonlinearities in fishnet metamaterials. *Sci. Rep.* **6**, 28440. (doi:10.1038/srep28440)
14. Melentiev PN, Afanasiev AE, Kuzin AA, Baturin AS, Balykin VI. 2013 Giant optical nonlinearity of a single plasmonic nanostructure. *Opt. Express* **21**, 13 896–13 905. (doi:10.1364/OE.21.013896)
15. Kruk S, Weismann M, Bykov AY, Mamonov EA, Kolmychek IA, Murzina T, Panoiu NC, Neshev DN, Kivshar YS. 2015 Enhanced magnetic second-harmonic generation from resonant metasurfaces. *ACS Photonics* **2**, 1007–1012. (doi:10.1021/acsp Photonics.5b00215)
16. Reinhold J *et al.* 2012 Contribution of the magnetic resonance to the third harmonic generation from a fishnet metamaterial. *Phys. Rev. B* **86**, 115401. (doi:10.1103/PhysRevB.86.115401)
17. Smirnova DA, Khanikaev AB, Smirnov LA, Kivshar YS. 2016 Multipolar third-harmonic generation driven by optically induced magnetic resonances. *ACS Photonics* **3**, 1468–1476. (doi:10.1021/acsp Photonics.6b00036)
18. Mie G. 1908 Beiträge zur Optik trüber Medien, speziell kolloidaler Metallösungen. *Ann. Phys. (Berlin)* **25**, 377–445. (doi:10.1002/andp.19083300302)
19. Ginn JC *et al.* 2012 Realizing optical magnetism from dielectric metamaterials. *Phys. Rev. Lett.* **108**, 097402. (doi:10.1103/PhysRevLett.108.097402)
20. Kuznetsov AI, Miroshnichenko AE, Fu YH, Zhang J, Luk'yanchuk B. 2012 Magnetic light. *Sci. Rep.* **2**, 492. (doi:10.1038/srep00492)
21. Evlyukhin AB, Novikov SM, Zywiets U, Eriksen RL, Reinhardt C, Bozhevolnyi SI, Chichkov BN. 2012 Demonstration of magnetic dipole resonances of dielectric nanospheres in the visible region. *Nano Lett.* **12**, 3749–3755. (doi:10.1021/nl301594s)
22. Kuznetsov AI, Miroshnichenko AE, Brongersma ML, Kivshar YS, Luk'yanchuk B. 2016 Optically resonant dielectric nanostructures. *Science* **354**, aag2472. (doi:10.1126/science.aag2472)
23. Dolgova TV, Mailykovski AI, Martemyanov MG, Fedyanin AA, Aktsipetrov OA, Marowsky G, Yakovlev VA, Mattei G. 2002 Giant microcavity enhancement of second-harmonic generation in all-silicon photonic crystals. *Appl. Phys. Lett.* **81**, 2725–2727. (doi:10.1063/1.1510968)
24. Martemyanov MG, Kim EM, Dolgova TV, Fedyanin AA, Aktsipetrov OA, Marowsky G. 2004 Third-harmonic generation in silicon photonic crystals and microcavities. *Phys. Rev. B* **70**, 073311. (doi:10.1103/PhysRevB.70.073311)
25. Leuthold J, Koos C, Freude W. 2010 Nonlinear silicon photonics. *Nature Photonics* **4**, 535–544. (doi:10.1038/nphoton.2010.185)
26. Shcherbakov MR *et al.* 2014 Enhanced third-harmonic generation in silicon nanoparticles driven by magnetic response. *Nano Lett.* **14**, 6488–6492. (doi:10.1021/nl503029j)
27. Shcherbakov MR *et al.* 2015 Ultrafast all-optical switching with magnetic resonances in nonlinear dielectric nanostructures. *Nano Lett.* **15**, 6985–6990. (doi:10.1021/acsnanolett.5b02989)
28. Shcherbakov MR *et al.* 2015 Nonlinear interference and tailorable third-harmonic generation from dielectric oligomers. *ACS Photonics* **2**, 578–582. (doi:10.1021/acsp Photonics.5b00065)
29. Shorokhov AS *et al.* 2016 Multifold enhancement of third-harmonic generation in dielectric nanoparticles driven by magnetic Fano resonances. *Nano Lett.* **16**, 4857–4861. (doi:10.1021/acsnanolett.6b01249)

30. Staude I *et al.* 2013 Tailoring directional scattering through magnetic and electric resonances in subwavelength silicon nanodisks. *ACS Nano* **7**, 7824–7832. (doi:10.1021/nm402736f)
31. Wang L *et al.* 2016 Multipolar third-harmonic generation in fishnet metamaterials. *ACS Photonics* **3**, 1494–1499. (doi:10.1021/acsp Photonics.6b00040)
32. Melentiev PN, Afanasiev AE, Kuzin AA, Gusev VM, Kompanets ON, Esenaliev RO, Balykin VI. 2016 Split hole resonator: a nanoscale UV light source. *Nano Lett.* **16**, 1138–1142. (doi:10.1021/acs.nanolett.5b04373)
33. Boyd RW 2003 *Nonlinear optics*, 2nd edn. San Diego, CA: Academic Press.